PERGAMON

International Journal of Solids and Structures 36 (1999) 4089–4109

INTERNATIONAL JOURNAL OF SOLIDS and STRUCTURES

A 3-D ellipsoidal flaw model for brittle fracture in compression

E. Z. Wang, N. G. Shrive*

Department of Civil Engineering, University of Calgary, Alberta, Canada T2N 1N4

Received 1 January 1998; in revised form 17 June 1998

Abstract

Engineering materials are rarely free of flaws. Mode I cracking from pre-existing flaws is the major cause of the brittle fracture in compression of materials such as concrete and rock. A 3-D ellipsoidal flaw model is used to show the significant influence of flaw geometry on crack initiation in uniform uniaxial, biaxial and triaxial compression. The model shows that the governing criterion for crack initiation may change from energy to stress with increasing crack size, and that for voids of similar size a spherical void is the most critical shape for crack initiation. The model thus provides a basis for a better understanding of both the phenomenon and the mechanism of brittle fracture in compression.

1. Introduction

Similar cracking patterns occur in similar uniaxial compression tests (Peng and Podnieks, 1972; Shrive and El-Rahman, 1985), biaxial compression tests (Vile, 1968; Brown 1974; Page, 1982) and triaxial compression tests (Bridgman, 1952; Hobbs, 1971) on different brittle and quasi-brittle materials. These experimental observations indicate that there must be a common fundamental cause of brittle fracture in compression. Hence, any theoretical model of compressive fracture should be applicable to all such materials.

It is generally accepted that the cause of fracture and failure of concrete is the proliferation of flaws or microcracks which exist within the body of the material even prior to the application of load (Kotsovos, 1979). Lajtai et al. (1990) pointed out that fracture starting from flaws should be fundamental to all investigations of brittle fracture. Since various flaw geometries such as cracks, pores, voids and fissures exist in materials, the influences of flaw geometry and flaw distribution on brittle fracture are critical. It should be noted that understanding of the fundamental fracture mechanism(s) in compression may be misled by perceptions based on some experimental obser-

* Corresponding author. Fax: 001 403 282 7026; E-mail: shrive@ucalgary.ca

0020–7683/99/$ - see front matter
PII: S0020–7683(98)00189–9

vations of artificial (man-made) 2-D inclined cracks subject to uniaxial compression. In uniaxial compression, a 2-D inclined crack kinks towards the direction of uniaxial compression. However, the 2-D slit crack model is unrealistic in that it does not predict crack propagation when the initial line of the zero width (or thickness) disk-like crack is parallel to the direction of the uniaxial compression: that is, when the 2-D slit crack is orientated precisely in the direction in which cracks propagate in uniaxial compression. In reality, multiple visible cracks parallel to the uniaxial compressive load are always seen: very few cracks emanating from angled slits are observed (Lajtai, 1974; Gol'dsthein et al., 1974). Indeed, Lajtai (1974) makes the point that what is created artificially is not seen in normal materials. Therefore, brittle fracture emanating from pre-existing 3-D pores or voids in compression has received considerable attention in the last decade (Sammis and Ashby, 1986).

Evans and Marathe (1968) investigated the effect of 2-D holes of various shapes on the tensile strength of plain concrete, whilst Raju (1970) examined the effect of stress concentrations produced by a circular hole on the static and fatigue strengths of concrete in uniaxial compression. Indeed, porosity, a measure of the number and size of finite width voids, has been described as the dominant controlling factor limiting the compressive strength of hardened cement past (Roy and Gouda, 1975). The presence of voids in concrete greatly reduces its compressive strength: 5% voids can lower compressive strength by as much as 30% compared to the strength of the same mix when fully compacted (Neville, 1981). Concrete researchers thus agree that air voids and microcracks inherently present in concrete have an important influence on the ultimate strength of the material (Kotsovos, 1979). Similarly, many physical properties of crystalline rocks are dramatically affected by the presence of voids, even though the void space may be less than 1% of the volume (Brace et al., 1972).

Undoubtedly, the flaws randomly distributed in a material are of extremely complicated shapes and are not in general, Griffith's line cracks. Zaitsev (1983) presented the observed frequency of different 2-D pore shapes in hardened cement paste and indicated the dominance of circular and elliptic shapes. Open cavities with cross-sections of various shapes have been observed in crystalline rocks with the majority of cavities nearly equant in cross-section: however, long, narrow, sharp-ended cracks were almost never seen in unstressed samples (Sprunt and Brace, 1974).

Various theoretical models have been developed to describe brittle fracture in compression. Zaitsev (1971) proposed a 2-D pore model for crack growth and failure of concrete and hardened cement paste under compressive load. Murrell and Digby (1970) and Paul and Mirandy (1976) independently developed a stress-based 'flat' ellipsoidal model. Using simple analytical results of fracture mechanics and beam theory, Sammis and Ashby (1986) analyzed the growth of axial cracks from 2-D cylindrical holes and from 3-D spherical pores in a compressive stress field. Madenci and Klemm (1992) and Madenci (1991) obtained the stress intensity factors for both an axial crack-like defect in a finite-width plate subject to in-plane uniaxial compression. Since a zero-width line crack model is unresponsive to normal stress coaxial to the crack direction, Yuan et al. (1993) proposed a 2-D finite-width elliptical crack model to derive the crack opening stress intensity factor. For two collinear radial cracks emanating from circular hole in a direction parallel to the direction of the applied compression, Dyskin et al. (1993) obtained the long crack asymptotic expressions for the stress intensity factor. The approximate method was also extended to a disk-like crack growing from the initial spherical pore in biaxial compression. In addition, a plane sliding crack model has been proposed (Nemat-Nasser and Horii, 1982) as well as others (Bazant

and Ozbolt, 1992). However, due to the complexity of the mathematical formulation, most of these contributions have been dimensionally limited or have been based on either a cohesive strength or an energy balance concept alone, which may restrict their general utility for different materials under various stress states. Further, although some models (e.g., phenomenological continuum damage models) were made to agree quite well with a particular set of measured experimental data through 'material constants', these models have had only limited success in providing an understanding of the mechanisms and processes of fracture in compression.

Most of the available test data on compressive strength are obtained from materials containing internal flaws and therefore, a direct application of the results of plane stress or plane strain analysis to these cases may not be valid. Slate (1983) pointed out that cracks on an exterior surface may be different from cracks in the interior of concrete and that conclusions about a mass of concrete based on surface observations only may be misleading or wrong. Crack extension from a 3-D flaw has been shown to be more complex than 2-D predictions (Adams and Sines, 1978). Therefore, an analytical study of the effect of 3-D ellipsoidal flaw geometry on crack initiation under uniform uniaxial, biaxial and triaxial compression was undertaken involving both a stress criterion and an energy criterion. The objective is to provide understanding of the processes and criteria for crack initiation from various pre-existing ellipsoidal flaws in compression.

2. A 3-D ellipsoidal flaw model

It is most unlikely that there is a sudden and substantial change in the criteria for brittle fracture as one traverses from tension to compression in stress space. Hence, the criteria for brittle fracture in compression will be similar to those in tension, even though different cracking patterns are observed in the different stress states. We therefore assume that Mode I (opening mode) cracking dominates brittle fracture under a general stress state and the governing criteria may be described as

(1) Stress criterion: local tensile stress developed around a flaw must be large enough to overcome the local cohesive strength of the material.
(2) Energy criterion: the energy released by a unit increment in the crack surface area must be at least as much as the energy required for that increment.

Note that there are fundamental differences in Mode I fracture due to tensile and compressive loads applied to the material. The relationship between the bond force and interatomic spacing (Van Vlack, 1989) indicates that interatomic or intramolecular bonds must be stretched to cause fracture: compressive stress cannot break the bond. This fact is exemplified vividly by loading a homogeneous material in hydrostatic compression. The tensile stress criterion cannot be satisfied (Shrive and El-Rahman, 1985), so no fracture occurs under the highest pressure which can be applied, even on brittle materials which otherwise appear weak: sometimes plastic behaviour occurs. For Mode I fracture to occur in a grossly compressive stress state, a local tensile stress must be created at the tip of a flaw in order to break interatomic bonds in the material.

It has been proposed in Wang and Shrive (1993) that crack initiation from a flaw occurs when both the stress and energy criteria are fulfilled simultaneously for the first time: stable or unstable propagation may follow. However, crack initiation and propagation may be governed by the stress

criterion or the energy criterion or both, and are dependent upon the material properties, the state of applied stress and the geometry of the flaw. Hence, to determine the governing criterion for fracture, both the stress and energy criteria should be considered. Here, the word 'crack' should be considered as terminology for various flaws.

A 3-D ellipsoidal flaw model has been proposed previously (Wang and Shrive, 1993). The ellipsoid is versatile enough to cover a wide range of flaw shapes and suitable to reflect the influence of flaw geometry on brittle fracture in compression. Six typical ellipsoidal shapes are illustrated in Fig. 1. The Cartesian coordinate axes, x, y and z are chosen so that they coincide with the directions

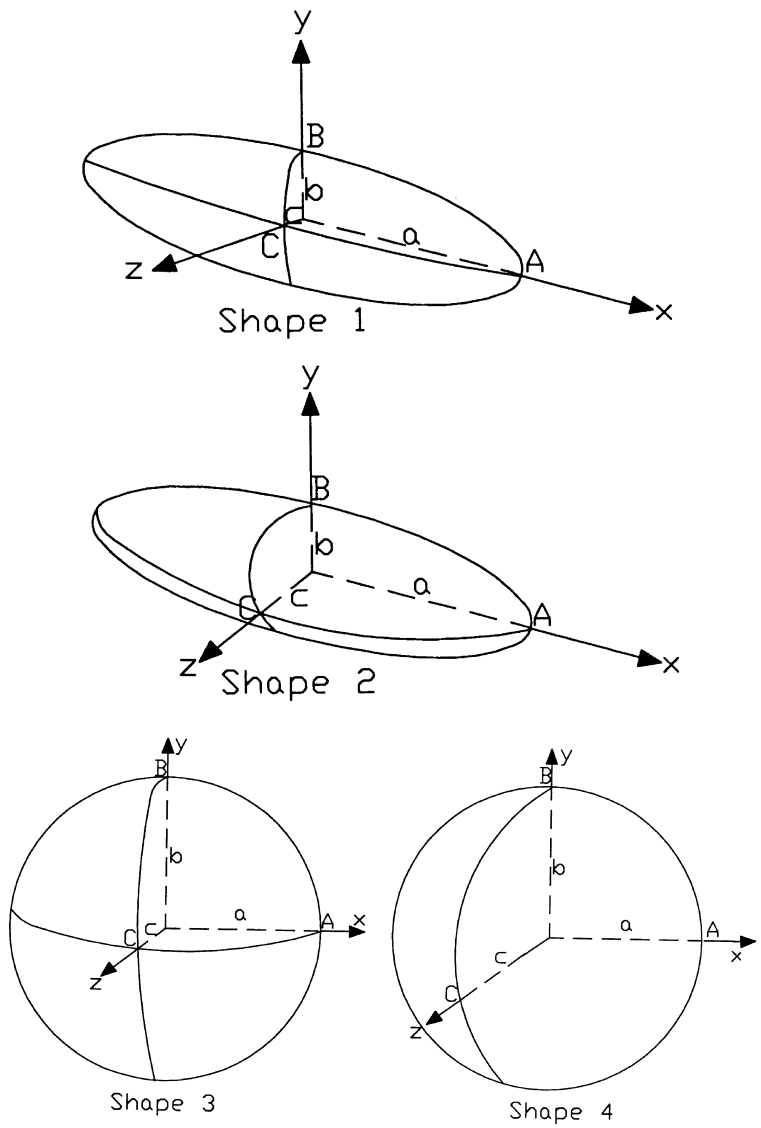

Fig. 1. Typical ellipsoidal shapes 1–6 and the Cartesian coordinate system.

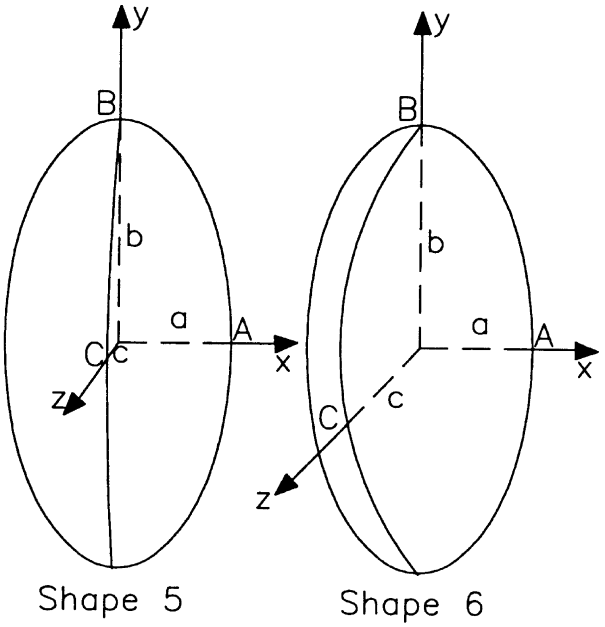

Fig. 1 continued.

of the principal semi-axes. These principal semi-axes are characterized by lengths a, b, and c. The points A, B and C are on the surface of the flaw where the principal stresses at infinity are σ_x^∞, σ_y^∞, and σ_z^∞ and their directions are restricted in the coordinate axes x, y and z. The stresses are treated as positive when tensile, negative when compressive. The body forces are neglected and the surface of the ellipsoid is assumed to be free from boundary stresses. The requirement that the principal semi-axes of the ellipsoid align with the applied principal stress directions is one limitation of the current 3-D model. Confining the surrounding infinite medium to being homogeneous, isotropic and linear elastic is another.

The analyses of the stress distributions and energy release rates for various flaws are fundamental to our understanding of the fracture process. For example, Savin (1961) investigated the stress concentration around various holes in a plane or plate. Peterson (1974) presented the charts of stress concentration factors for some special ellipsoidal shapes under uniaxial or biaxial stresses at infinity, e.g., $b = c$ or $a = b = c$. Various approaches to the calculation of stress concentrations have been extensively reviewed by Durelli (1981).

For our model, a closed-form solution for the stress distribution σ_{ij}^c, around a 3-D ellipsoidal void embedded in an infinite medium subject to uniform stresses σ_x^∞, σ_y^∞ and σ_z^∞ at infinity was given Sadowsky and Sternberg (1949). In the orthogonal ellipsoidal coordinates, the complete stress solution, σ_{ij}^c, can be expressed as a linear combination of the stress field σ_{ij}^∞, and the five stress component solutions $(\sigma_{ij})_N$. This is

$$\sigma_{ij}^c = \sigma_{ij}^\infty + \sum_{N=1}^{5} A_N(\sigma_{ij})_N \quad (i,j = 1,2,3), \tag{1}$$

where the coefficients A_N are determined by the boundary conditions on the surface of the flaw, see Sadowsky and Sternberg (1949). The calculation of the stress distribution around an ellipsoidal void has been implemented into a computer code and validated by El-Rahman (1983).

The energy release rate G_I is defined by

$$G_I = \frac{\partial U}{\partial S} = \lim_{\Delta S \to 0} \frac{\Delta U}{\Delta S} \tag{2}$$

in which ΔU represents the energy released due to the newly formed surface area of the void, ΔS. It is very difficult to predict the exact profile of the real crack extension from an ellipsoidal void under a given stress state, since an infinite number of virtual crack extensions could be used to calculate the energy release rate. However, if the stress criterion is satisfied for a number of virtual crack extensions, the most likely crack extension is the one which makes the energy release rate a maximum of all the values produced by these virtual crack extensions. Here, to calculate the 'initial' energy release rate at the moment of crack initiation from an ellipsoidal void, as shown in Fig. 1, a virtual crack extension is assumed to be generated by a certain combination of da, db and dc, i.e., the positive infinitesimal increments of a, b and c. Only those increments occur which are perpendicular to the direction of the maximum tensile stress at the tips of the void and the zone of tension. Thus if σ_2 at A and B is the biggest tensile stress, only a and b are increased: dc is zero. As a result, in this model, an initial ellipsoidal void is enlarged into a differently shaped ellipsoidal void depending on which of a, b and c are incremented. Essentially the new void is created by the removal of material from the medium. This selective material removal is deemed to be a virtual crack extension. G_I is estimated from

$$G_I = \frac{\Delta U}{\Delta S} \tag{3}$$

in which ΔS is the difference in the surface area of the new void compared to the original void

$$\Delta S = S(a + \mathrm{d}a, b + \mathrm{d}b, c + \mathrm{d}c) - S(a, b, c), \tag{4}$$

and ΔU is the difference in the energy reduction due to the presence of the new void, compared to the original void.

$$\Delta U = U(\sigma_x^\infty, \sigma_y^\infty, \sigma_z^\infty, E, \mu, a + \mathrm{d}a, b + \mathrm{d}b, c + \mathrm{d}c) - U(\sigma_x^\infty, \sigma_y^\infty, \sigma_z^\infty, E, \mu, a, b, c). \tag{5}$$

Since no singularities exist in the stress and strain components around an ellipsoidal void with finite width subject to compression, a 'strain method' developed in Wang and Shrive (1994) is used to calculate the energy release rate. To show the accuracy of U and G_I calculated by the strain method, a spherical void with radius R, embedded in an infinite medium subject to uniform stresses σ_x^∞, σ_y^∞, and σ_z^∞ at infinity is taken as an example. For a spherical void, the stress components at points A, B and C in the x-, y- and z- directions can be derived from the analysis of Southwell and Gough (1926). For example at point B:

$$(\sigma_x)_B = (\sigma_{33}^c)_B = \frac{3}{14 - 10\mu}\left[(9 - 5\mu)\sigma_x^\infty - (1 + 5\mu)\sigma_y^\infty - (1 - 5\mu)\sigma_z^\infty\right], \tag{6}$$

$$(\sigma_y)_B = (\sigma_{11}^c)_B = 0, \tag{7}$$

$$(\sigma_z)_B = (\sigma^c_{22})_B = \frac{3}{14-10\mu}\left[-(1-5\mu)\sigma_x^\infty - (1+5\mu)\sigma_y^\infty + (9-5\mu)\sigma_z^\infty\right]. \tag{8}$$

Thus, we have

$$(\varepsilon_x)_B = \frac{3}{(14-10\mu)E}\left[(9-4\mu-5\mu^2)\sigma_x^\infty - (1+4\mu-5\mu^2)\sigma_y^\infty - (1+4\mu-5\mu^2)\sigma_z^\infty\right], \tag{9}$$

$$(\varepsilon_y)_C = \frac{3}{(14-10\mu)E}\left[-(1+4\mu-5\mu^2)\sigma_x^\infty - (9-4\mu-5\mu^2)\sigma_y^\infty - (1+4\mu-5\mu^2)\sigma_z^\infty\right], \tag{10}$$

$$(\varepsilon_z)_B = \frac{3}{(14-10\mu)E}\left[-(1+4\mu-5\mu^2)\sigma_x^\infty - (1+4\mu-5\mu^2)\sigma_y^\infty - (9-4\mu-5\mu^2)\sigma_z^\infty\right]. \tag{11}$$

A simple equation presented by Wang and Shrive (1994) provides the change in the total potential energy of the infinite medium and the applied load due to the presence of a spherical void. This is

$$U = \frac{2}{3}\pi abc\left[\sigma_x^\infty(\varepsilon_x)_B + \sigma_y^\infty(\varepsilon_y)_C + \sigma_z^\infty(\varepsilon_z)_B\right]. \tag{12}$$

Substituting eqns (9), (10), and (11) into eqn (12), we find

$$U = \frac{\pi(1-\mu)R^3}{(7-5\mu)E}\{(9+5\mu)[(\sigma_x^\infty)^2 + (\sigma_y^\infty)^2 + (\sigma_z^\infty)^2] - 2(1+5\mu)(\sigma_x^\infty\sigma_y^\infty + \sigma_x^\infty\sigma_z^\infty + \sigma_y^\infty\sigma_z^\infty)\}. \tag{13}$$

Assuming that a spherical void with radius R virtually extends into a bigger spherical void with radius $R+\mathrm{d}R$, we can obtain an 'artificial' G_I, i.e.,

$$G_I = \frac{\mathrm{d}U}{\mathrm{d}R}\frac{\mathrm{d}R}{\mathrm{d}S} = \frac{3(1-\mu)R}{8(7-5\mu)}\{(9+5\mu)[(\sigma_x^\infty)^2 + (\sigma_y^\infty)^2 + (\sigma_z^\infty)^2] - 2(1+5\mu)(\sigma_x^\infty\sigma_y^\infty + \sigma_x^\infty\sigma_z^\infty + \sigma_y^\infty\sigma_z^\infty)\}. \tag{14}$$

in which $S = 4\pi R^2$. For comparison, both the numerical values with $c = 0.99$ $b \approx b = 0.99a \approx a = R = 10$ and the exact values obtained from the above explicit equations are presented in Tables 1 and 2. Young's modulus $E = 1$. In the numerical calculation of G_I,

Table 1
U for a spherical void subject to compression

	Uniaxial compression		Biaxial compression		Triaxial compression	
	$\sigma_y^\infty = -1, \sigma_x^\infty = \sigma_z^\infty = 0$		$\sigma_x^\infty = \sigma_y^\infty = -1, \sigma_z^\infty = 0$		$\sigma_x^\infty = \sigma_y^\infty = \sigma_z^\infty = -1$	
	$\mu = 0.2$	$\mu = 0.3$	$\mu = 0.2$	$\mu = 0.3$	$\mu = 0.2$	$\mu = 0.3$
Numerical	4064.3	4073.5	6480.7	6182.2	7316.2	6401.8
Equation (13)	4188.8	4198.3	6702.1	6397.4	7539.8	6597.3

Table 2
G_I for a spherical void (increasing uniformly in R in all directions) subject to compression

	Uniaxial compression		Biaxial compression	
	$\sigma_y^\infty = -1, \sigma_x^\infty = \sigma_z^\infty = 0$		$\sigma_x^\infty = \sigma_y^\infty = -1, \sigma_z^\infty = 0$	
	$\mu = 0.2$	$\mu 2 = 0.3$	$\mu = 0.2$	$\mu = 0.3$
Numerical	4.9500	4.9613	7.9019	7.5396
Equation (14)	5.0000	5.0114	8.0000	7.6364

$da = db = dc = 0.0001$. The relative errors between the numerical and exact values are less than 3.4% for U and less than 1.3% for G_I. Note that the virtual crack extension used to validate the computer code (R increasing by dR in all directions) is unlikely to occur in practice.

A common assumption in fracture models is that the possible crack extension direction is along a plane perpendicular to the direction of the maximum tensile stress developed around the crack. We make that assumption in this ellipsoidal void model and also assume that the material associated with the virtual crack extension is removed from the infinite medium to form the new configuration of the void, as assumed in Rice and Drucker (1967). It should be noted that in compression, the void front opens up through the action of a local tensile stress zone at the tips of the void with tensile σ_{max}. For example, the tensile σ_{max} exists at point B (Fig. 1) in the z-direction for an ellipsoidal void with $a > c$ under compressive stress σ_y^∞. If we assume in this case that only two principal semi-axes, a and b, change with crack propagation while the third principal semi-axis, c, does not, G_I can be expressed as

$$G_I = \frac{\frac{\partial U}{\partial a}da + \frac{\partial U}{\partial b}db}{\frac{\partial S}{\partial a}da + \frac{\partial S}{\partial b}db}. \tag{15}$$

There are an infinite number of virtual crack extensions, i.e., various combinations of da and db, to generate various values of G_I. However, G_I has two bounds, i.e., a maximum and a minimum of G_I defined by eqn (15), corresponding to the following two special cases. They are
Case 1: (upper bound) $da > 0$ and $db = 0$.

$$G_I = \frac{\frac{\partial U}{\partial a}}{\frac{\partial S}{\partial a}}. \tag{16}$$

Case 2: (lower bound) $da = 0$ and $db > 0$.

$$G_{\mathrm{I}} = \frac{\dfrac{\partial U}{\partial b}}{\dfrac{\partial S}{\partial b}}. \tag{17}$$

From the point of view of energy, crack extension tends to release as much energy as possible. However, the stress criterion for the associated crack extension must be satisfied. For the above example since $\mathrm{d}a = 0$ and $\mathrm{d}b > 0$ at the moment of crack initiation from point B, the 'initial' G_{I} is the lower bound.

To calculate the 'initial' energy release rates for the ellipsoidal voids in the following sections, we use principal semi-axes a, b, and c (not greater than 10), with $\mathrm{d}b = 0.0001$ (sufficiently small compared to 10) and $\mathrm{d}a = \mathrm{d}c = 0$ when the tensile $\sigma_{\max}$ is at point B in the z-direction and $\mathrm{d}b = \mathrm{d}c = 0$ when the tensile $\sigma_{\max}$ is at point B in the z-direction, and $da = 0.0001$ and $\mathrm{d}b = \mathrm{d}c = 0$ when the tensile $\sigma_{\max}$ is at point A in the z-direction. However, after crack initiation occurs at point B for example, $\mathrm{d}a > 0$ may also occur due to stress redistribution. For crack propagation from point B, it is reasonable to expect that $\mathrm{d}a < \mathrm{d}b$ and G_{I} is thus unlikely to reach its upper bound ($\mathrm{d}a > 0$ and $\mathrm{d}b = 0$). We therefore impose a 'lower' upper bound on G_{I} during fracture, estimated by $\mathrm{d}a = \mathrm{d}b = 0.0001$ and $\mathrm{d}c = 0$. A similar set of arguments can be made for propagation from point A.

Since a, b and c are assumed to be ordered by $a > b > c > 0$ in (Sadowsky and Sternberg, 1949), we remove this order in the following discussions through automatic switching in the computer code of the principal axes and the applied principal stresses at infinity to take a, b and c to be the large, middle and small principal semi-axes of an ellipsoid, respectively. Special ellipsoidal shapes, i.e., $a = b$ and/or $a = c$ and/or $b = c$, are treated as the limiting shapes and given approximately by $b = 0.99\ a \approx a$ and/or $c = 0.99\ b \approx b$. Tables 1 and 2 indicate that such approximations will produce reliable and stable numerical results for special shapes.

3. Results and discussion

Three sequential events are frequently discussed in the fracture of brittle materials subject to compression: crack initiation, crack propagation and the coalescence of cracks leading to the final failure. Here, we focus on crack initiation and consider pre-existing flaws as the leading source of cracking.

The classic Griffith's line crack subject to tension normal to the crack plane is represented only by its length. However, for a general 2-D or 3-D flaw, not only the size but the shape is an important factor affecting crack initiation and propagation. Lajtai (1971) found experimentally that in uniaxial compression for all elliptical shapes, the major axis of the critically oriented open crack is perpendicular to the direction of the uniaxial compression, and an open circular hole becomes the 'critical shape' as long as its diameter is not smaller than the maximum dimension of all open elliptical cracks having any orientation and shape. Here, to show how 3-D ellipsoidal geometry affects both the maximum tensile stress and the energy release rate under uniform uniaxial, biaxial and triaxial compression, the dominant, maximum principal semi-axis of ellipsoids is set arbitrarily. Further, since our ellipsoidal flaw model fails physically to estimate the energy

Table 3
σ_{max} and G_I of ellipsoidal shapes 1–6 in uniaxial compression

Shape		1	2	3	4	5	6
$\mu = 0.2$	σ_{max}	0.9782	0.9545	0.6262	0.5029	0.2701	0.2723
	G_I	0.0336	0.3986	0.0332	2.0082	0.0327	0.2072
		(0.0341*)	(0.4351*)	(0.0336*)	(4.1797*)	(0.0339*)	(0.4063*)
$\mu = 0.3$	σ_{max}	0.9844	0.9742	0.7167	0.6838	0.4450	0.4546
	G_I	0.0336	0.4047	0.0332	2.0893	0.0327	0.2070
		(0.0341*)	(0.4366*)	(0.0336*)	(4.2079*)	(0.0339*)	(0.4077*)

* Values calculated by $da = db = 0.0001$.

release rate for flaws with $a > b$ and $c > b$ subject to a dominant compressive stress σ_y^∞ and because crack initiation from these flaws appears to be physically impossible in our model, since crack propagation is assumed to be a 'growing' ellipsoid by removal of material. Only six typical flaw shapes in the ellipsoidal family are examined. Dimensionless values are assigned to a, b, and c, respectively, for the following normalized comparisons with respect to Young's modulus, i.e., $E = 1$.

Shape 1: $a = 10$, $b = 1$ and $c = 0.1$ ($a > b > c$).
Shape 2: $a = 10$, $b = 1$ and $c = 1$ ($a > b = c$).
Shape 3: $a = 10$, $b = 10$ and $c = 0.1$ ($a = b > c$).
Shape 4: $a = 10$, $b = 10$ and $c = 10$ ($a = b = c$).
Shape 5: $a = 1$, $b = 10$ and $c = 0.1$ ($b > a > c$).
Shape 6: $a = 1$, $b = 10$ and $c = 1$ ($b > a = c$).

The above ellipsoidal shapes 1–6 are illustrated in Fig. 1. The differences among the principal semi-axes, a, b and c for the above applicable shapes are expected to represent the extreme of typical flaw shapes. Although shape 4 is approximated by a limiting shape in our computer code, for simplicity this shape will still be called spherical in the following discussion of the numerical results.

3.1. Uniaxial compression

A unit uniaxial compressive stress is applied in the y-direction, i.e., $\sigma_y^\infty = -1$. The numerical results for σ_{max} and G_I for the six void shapes are presented in Table 3. The pre-existing flaws change the state of stress in the material from 'global' compression to 'local' tension and result in Mode I cracking. The tensile σ_{max} is always at point B in the z-direction. σ_{max} occurs in the z-direction rather than any other direction for shapes 4 and 6 because of the required numerical approximation $c = 0.99a \approx a$. This tension explains the observed cracking in specimens, parallel to the applied uniaxial compressive stress (Shrive and El-Rahman, 1985). Myer et al. (1992) found that in Indiana limestone under uniaxial compression, many cracks originated at pores as a result of tensile stresses tangential to the pore boundaries. Chao and Van Vlack (1965) observed cracks

develop above and below soft particles embedded in a sintered steel matrix under uniaxial compressive load. The conical, pyramidal, or wedge-shaped pieces frequently observed at the platens after specimen failure in typical 'uniaxial' compression tests are due to the lateral confining effect of the loading platens of the test machine. These shapes develop from angled principal stresses caused by shear between specimen and platen and are a secondary or 'post-cracking' effect.

Both $\sigma_{\max}$ and G_{I} are quite sensitive to the ellipsoidal shapes. If a material contains flaws with shapes 1–6 which have little tendency to close in compression, it is of great interest for engineering practice to find the most 'critical shape' flaw which generates crack initiation under the lowest applied stress. Based on the criteria for Mode I crack initiation, shape 4, the spherical void, is the most critical shape of voids of similar size to cause fracture in uniaxial compression. Since tensile $\sigma_{\max}$ always exists at point B in the z-direction, it could be expected that $\mathrm{d}a < \mathrm{d}b$ during fracture. Thus, 'lower' upper bounds can be obtained for shapes 1–6. Table 3 indicates a small difference between the initial G_{I} and the lower upper bound G_{I} for shapes 1, 2, 3 and 5, and an apparent difference for shapes 4 and 6. This indicates that if the change in the crack geometry for a short distance of propagation is ignored, G_{I} may increase during propagation for a pre-existing spherical void and an associated short extension is thus unstable at constant applied stress.

The stress concentrations at points A, B and C only depend on the shape of the void, but are not influenced by the absolute size of the void. Thus, fracture models based on a stress criterion only cannot be expected to explain the effect of flaw size (Lajtai, 1971; Carter et al. 1992). However, the energy criterion does account for the size of the void. Lajtai (1971) and Carter (1992) found in uniaxial compression tests, that the fracture initiation stress decreases with increasing cylindrical hole size and appears to approach a horizontal asymptote for large hole sizes. There are several theoretical models to explain the size effect and the accompanying strength anomalies (Carter, 1992). However, based on both a stress criterion and an energy criterion, our 3-D ellipsoidal flaw model may show the flaw size effect physically and logically. For example, different applied compressive stresses σ_y^{∞} at infinity are required for varying sizes of spherical void to provide the same G_{I} or tensile $\sigma_{\max}$ as the 'original' size of spherical void (radius $R = 10$ embedded in an infinite medium subject to compressive stress σ_{yo}^{∞} at infinity). The influence of the size of the spherical void on $\sigma_y^{\infty}/\sigma_{yo}^{\infty}$ for $\mu = 0.3$ is shown in Fig. 2. Note that the radius of the 'original' spherical void is arbitrarily chosen, and that both the stress and energy criteria are assumed to be satisfied simultaneously for crack initiation for this void subject to compressive stress σ_{yo}^{∞}. It can be seen that the size effect is pronounced in the small radius range with fracture dictated by the energy criterion: as the radius, R, approaches zero, the applied compressive stress required to cause Mode I fracture tends to be infinite. The results also suggest that the governing criterion for crack initiation may shift from the energy criterion to the stress criterion at some large radius. For other ellipsoidal flaws with specified shape, variations of $\sigma_y^{\infty}/\sigma_{yo}^{\infty}$ with flaw size have trends similar to those shown in Fig. 2. Lajtai (1974) found that by increasing the major axis of an open elliptic hole experimentally, whilst keeping the ratio of minor to major axis constant, the critical orientation for crack initiation shifts from being just about perpendicular to the direction of the uniaxial compression to being on an inclined orientation. This may indicate the shift of the governing criterion for crack initiation in compression with increasing flaw size.

Table 3 and Fig. 2 indicate that at a certain level of compressive loading, crack initiation may occur only from large and favourably shaped flaws. In geology, the influence of the size of flaws is of great importance. Geological structures that may act as flaws range in size from the atomistic

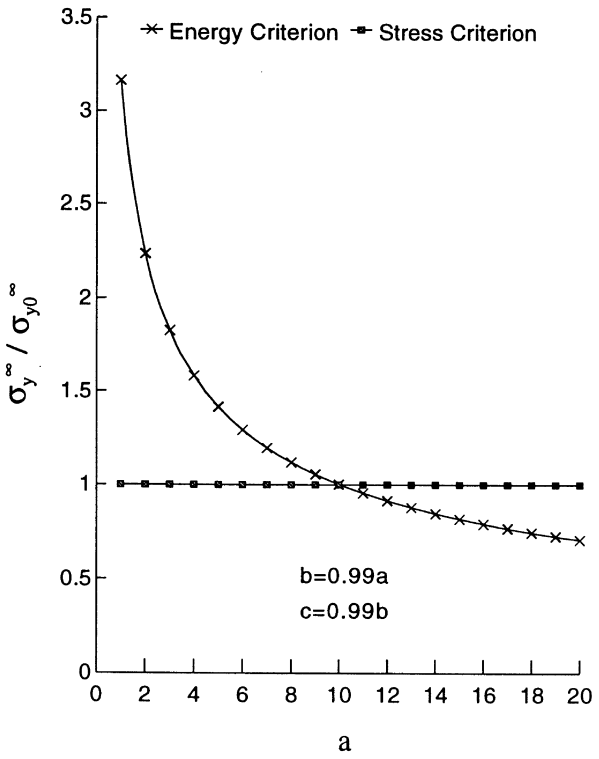

Fig. 2. Variation of crack initiation stress with size for a spherical void under uniaxial compression, with both criteria normalized against the value at $R = 10$.

(crystal defects) through microscopic (e.g., grain boundaries) and macroscopic (e.g., bedding and jointing) to megascopic (faults) (Lajtai, 1974). In concrete, pre-existing flaws are of different sizes and shapes (Neville, 1981) and large pores have the greatest influence on the compressive strength (Kumar, 1986). Many flaws are too small to cause fracture on the basis of the energy criterion. Theoretically, no Mode I cracking would occur in the material if all flaw sizes and/or the applied compressive stress were small enough so that the critical energy release rate of the material was not reached. Birchall et al. (1981) found that removal of 'large' voids to give macro-defect-free cements produced both high compressive (200 MPa) and high flexural (60–70 MPa) strengths. On the other hand, since very large cavities (e.g., underground openings) subject to compression may satisfy the energy criterion automatically, the stress criterion may govern the failure process. In such cases, simple stress-based design criteria may be reliable for engineering practice.

Note that the model used here predicts that the plane crack of zero width employed in some existing models for brittle fracture in compression results in no energy release as the crack grows parallel to the uniaxial compressive load. In reality, multiple visible cracks parallel to the uniaxial compressive load are always seen. In this context, our 3-D ellipsoidal flaw model with finite width satisfies basic thermodynamic and energy requirements, and concurs with experimental observations.

Table 4
σ_{max} and G_I of ellipsoidal shapes 1–6 in biaxial compression ($\sigma_y^\infty = -1$, $\sigma_x^\infty = -0.5$)

Shape		1	2	3	4	5	6
$\mu = 0.2$	σ_{max}	0.9875	0.9593	0.8089	0.5047	0.6142	0.4869
	G_I	0.0353	0.4205	0.0350	2.8918	0.0359	0.4555
		(0.0358*)	(0.4553*)	(0.0353*)	(4.5243*)	(0.0357*)	(0.4337*)
$\mu = 0.3$	σ_{max}	0.9914	0.9767	0.8558	0.6184	0.6929	0.4921
	G_I	0.0320	0.3839	0.0317	2.6996	0.0326	0.4155
		(0.0325*)	(0.4175*)	(0.0320*)	(4.2930*)	(0.0323*)	(0.3958*)

* Values calculated by $da = db = 0.0001$.

3.2. Biaxial compression

Based on the above uniaxial compression $\sigma_y^\infty = -1$, a lateral compressive stress σ_x^∞ is also applied to examine crack initiation in biaxial compression. We consider the following two cases.
Case 1: $\sigma_{y=-1}^\infty$ and $\sigma_x^\infty = -0.5$

In this case, the calculated results are listed in Table 4. The tensile σ_{max} is at point B in the z-direction for shapes 1–5 and at point A in the z-direction for shape 6. Thus, the biaxial failure mode can be expected as tensile splitting along a plane parallel to the free or unrestrained surface as observed experimentally (Vile, 1968; Brown, 1974; Page, 1982). From Table 4, we can see that again, the spherical void (shape 4) is the most critical shape for crack initiation from voids of similar size. Note that only shape 4 has an apparent difference between the initial G_I and the lower upperbound G_I. This indicates that if the change in the crack geometry for a short distance of propagation is ignored, a short unstable propagation from a pre-existing spherical void may occur at constant applied stresses.
Case 2: $\sigma_y^\infty = \sigma_x^\infty = -1$

Because of the symmetry in this case, only four shapes are taken into account for the comparison. The values of σ_{max} and G_I are given in Table 5 and the tensile σ_{max} is at point B in the z-direction for all shapes. Table 5 reveals that shape 4 is again the most critical shape for crack initiation. Except for the maximum tensile stress for shape 4 with $\mu = 0.3$, both σ_{max} and G_I increase in equal biaxial compression, i.e., $\sigma_y^\infty = \sigma_x^\infty = -1$, compared to uniaxial compression (i.e., $\sigma_y^\infty = -1$, presented in Table 3). In addition, shapes 1 and 2 have small differences between the initial G_I and the lower upper bound G_I, whereas for shapes 3 and 4, a unique value of G_I for various virtual crack extensions should be obtained, due to the coincidence of the lower and upper bounds. From the point of view of energy, the spherical void would extend into an ellipsoidal void of uncertain shape.

Assuming that either the stress criterion or the energy criterion controls crack initiation in biaxial compression, we may determine what combination of stresses σ_y^∞ and σ_x^∞ is necessary to produce the required tensile stress or energy release rate for crack initiation. If $\sigma_x^\infty/\sigma_{ui}^\infty$ is varied between 0 and -1 in steps of 0.1, a series of values $\sigma_x^\infty/\sigma_{ui}^\infty$ can be determined for shapes 2 and 4. σ_{ui}^∞ is a generalized notation, which stands for the required uniaxial compressive stress to cause

Table 5
σ_{max} and G_I of ellipsoidal shapes 1–4 in biaxial compression ($\sigma_y^\infty = \sigma_x^\infty = -1$)

Shape		1	2	3	4
$\mu = 0.2$	σ_{max}	0.9969	0.9641	0.9934	0.5066
	G_I	0.0541	0.6551	0.0538	6.9485
		(0.0545*)	(0.6786*)	(0.0538*)	(6.9554*)
$\mu = 0.3$	σ_{max}	0.9985	0.9792	0.9950	0.5531
	G_I	0.0473	0.5865	0.0471	6.4721
		(0.0478*)	(0.6022*)	(0.0471*)	(6.4787*)

* Values calculated by $da = db = 0.0001$.

Mode I crack initiation for a specific shape and a specific Poisson's ratio on the basis of either the stress criterion or the energy criterion. The predicted crack initiation loci for shapes 2 and 4 when governed in one case by the stress criterion and the other by the energy criterion are shown in Figs 3–6, respectively. Note that σ_{ui}^∞ in Figs 3–6 for different Poisson's ratios, different shapes of flaws, different control criteria, the lower bounds of G_I and the 'lower' upper bounds of G_I are not necessarily the same values. In Fig. 4, for shape 2, if $\sigma_x^\infty/\sigma_{ui}^\infty$ is increased further to exceed 1, the maximum tensile stress may exist at point A rather than point B and such a case is the same as shape 6 in biaxial compression. For a spherical void, the crack initiation locus governed by the energy criterion should be symmetrical about the bisector of the first octant of the coordinate system in Fig. 6. Since the spherical shape is treated as a limiting shape in the ellipsoidal family by our computer code as mentioned before, the crack initiation loci shown in Fig. 6 are not perfectly symmetrical, as expected. Figures 4 and 6 show that a small difference for shape 2 and an apparent difference for shape 4 between the initial G_I and the lower upper bound or the upper lower bound G_I. this indicates that for the spherical void in biaxial compression, the crack initiation loci with the same initial G_I and the initial crack propagation loci with the same 'propagating' (but quasi-static) G_I may be quite different.

From the point of view of the energy criterion, it appears that biaxial compression for these shapes in general promotes Mode I crack initiation, which contradicts typical experimental findings (Kupfer et al., 1969; Brown, 1974, and many others) that the strengths of concrete and rocks under biaxial compression are higher than those under uniaxial compression. However, the crack initiation locus for shape 4 with $\mu = 0.3$ predicted by the stress criterion tends to confirm experimental findings. This indicates that if the grossly applied stress state varies from uniaxial compression to biaxial compression, the governing criterion for crack initiation may shift from the energy criterion to the stress criterion. Further, if a lateral compressive stress is applied in the other direction, e.g., $\sigma_z^\infty = -0.5$, a reversed result for some shapes is obtained as shown in Table 6. For shapes 1, 3, 5 and 6, the tensile, σ_{max} is at point C in the x-direction, while for shapes 2 and 4, the tensile σ_{max} is at point B in the x-direction. From the point of view of the stress criterion, it seems more difficult for Mode I cracking to initiate from shapes 1–3 flaws in biaxial compression

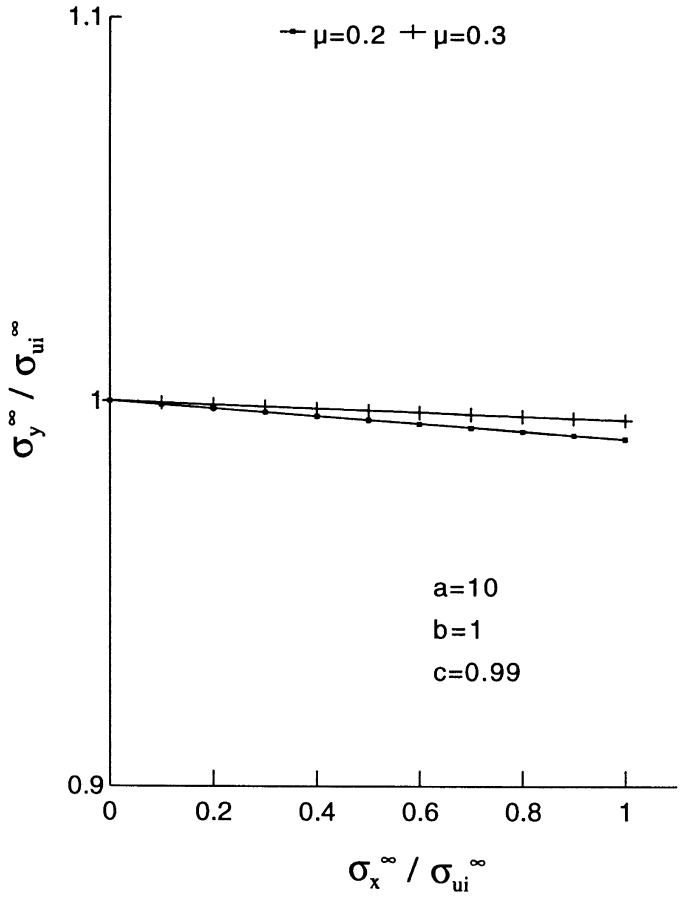

Fig. 3. Crack initiation loci governed by the stress criterion for shape 2 under biaxial compression.

than in uniaxial compression. Furthermore, compressive stress σ_z^{∞} may close shape 1, 3 and 5 flaws because c is much less than a and b.

The mechanisms of meso-scopic crack initiation as discussed here, and final macro-failure in compression may be different. However, initial crack propagation is necessary for final failure, so the mechanisms should not be completely independent. Murrell and Digby (1970) pointed out that the initiation of crack propagation is not, in general, synonymous with the complete (macroscopic) fracture of a brittle body. This implies that the crack initiation loci of a single flaw may be dissimilar to the failure or strength loci of the material. Interestingly, some damage models (Mazars, 1986) indicate that micro- and meso-cracking processes in biaxial compression usually occur more easily than in uniaxial compression. The strength or final failure loci of brittle materials in biaxial compression tests may not provide a valid and proper test of the current model for initial crack propagation from a single flaw: 'Specimen' responses may not be the same as the underlying 'material' responses. Failure loci or strength envelopes for multiaxial stress states take various forms, depending on the specimen geometry, the specimen boundary conditions, distribution of

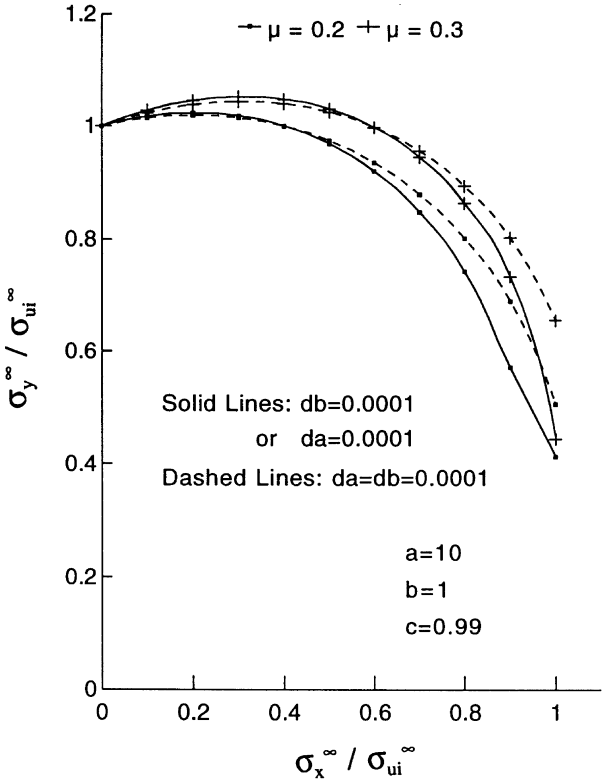

Fig. 4. Crack initiation loci governed by the energy criterion for shape 2 under biaxial compression.

flaws, material properties, loading rate and so on. The specimen/test machine interface is critical since it induces varying amounts of restraining stresses in the specimen near the ends, even when brush platens are used, thus affecting the deformation, compressive strength and final failure pattern of the specimen under test.

3.3. Triaxial compression

Concrete and rock are frequently loaded in triaxial stress states. Thus, it is of interest to examine what the model predicts will happen in triaxial compression.

An axial stress $\sigma_y^\infty = -1$ is applied with equal small orthogonal lateral stresses $\sigma_x^\infty = \sigma_z^\infty = -0.1$.

The numerical results presented in Table 7 show that the third stress plays a significant role in inhibiting crack initiation. No tensile stress exists in triaxial compression for shape 2 when $\sigma_x^\infty = \sigma_z^\infty \leqslant -0.32$ with $\mu = 0.2$ and -0.38 with $\mu = 0.3$; for shape 4 when $\sigma_x^\infty = \sigma_z^\infty \leqslant -0.25$ with $\mu = 0.2$ and -0.31 with $\mu = 0.3$; and for shape 6 when $\sigma_x^\infty = \sigma_z^\infty \leqslant -0.11$ with $\mu = 0.2$ and -0.16 with $\mu = 0.3$. If flaws shaped only like these existed in a brittle material, failure modes other than Mode I cracking would be expected to occur in triaxial compression. Hobbs (1971) for example,

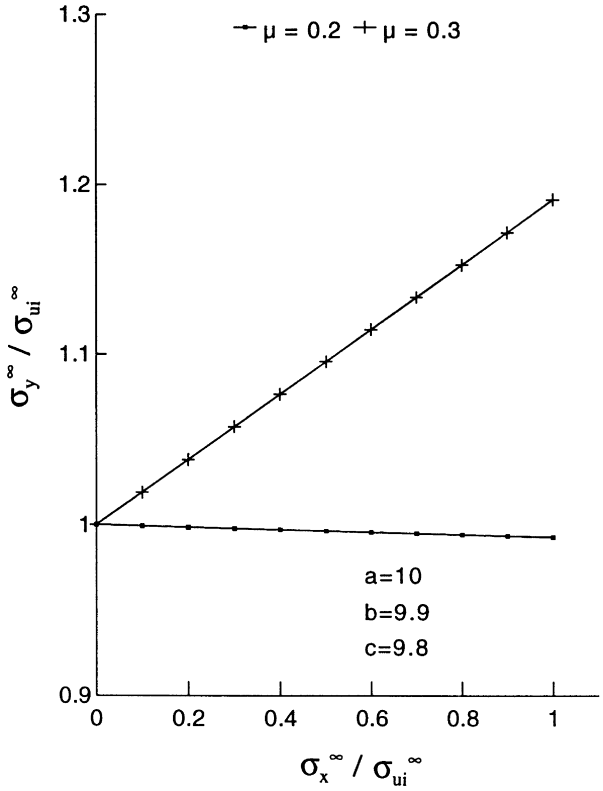

Fig. 5. Crack initiation loci governed by the stress criterion for shape 4 under biaxial compression.

Table 6
σ_{max} of ellipsoidal shapes 1–6 in biaxial compression ($\sigma_y^\infty = -1$, $\sigma_z^\infty = -0.5$)

Shape		1	2	3	4	5	6
σ_{max}	$\mu = 0.2$	0.1689	0.2222	0.3451	0.4953	0.4906	0.4866
	$\mu = 0.3$	0.2473	0.3249	0.3954	0.6088	0.4939	0.4919

found that the amounts of 'plastic flow' in concrete specimens increased substantially with increasing confining pressure.

4. Conclusions

The above comparisons indicate that the 3-D flaw geometry must be an important consideration for any theory of brittle fracture in compression. Mode I crack initiation appears to occur only

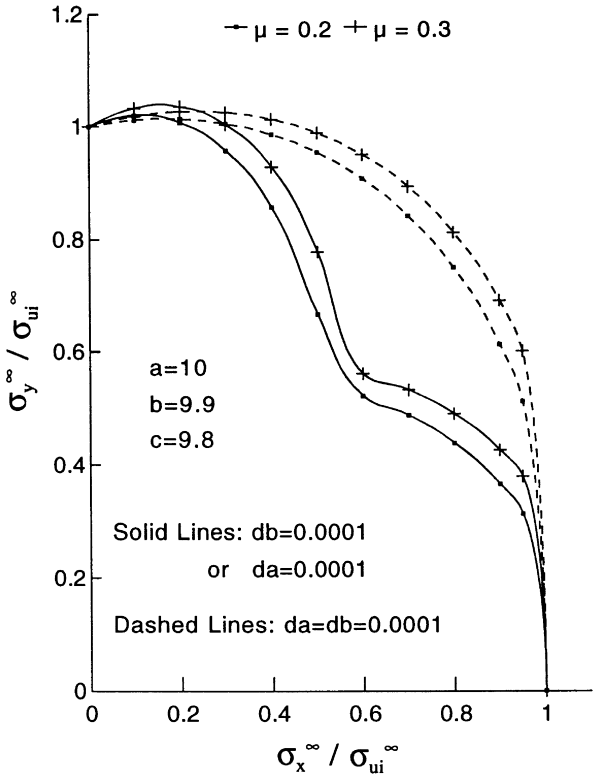

Fig. 6. Crack initiation loci governed by the energy criterion for shape 4 under biaxial compression.

Table 7
σ_{max} and G_I of ellipsoidal shapes 1–6 in triaxial compression

Shape		1	2	3	4	5	6
$\mu = 0.2$	σ_{max}	0	0.6602	0	0.3014	0	0.0253
	G_I	—	0.3333	—	1.8226	—	0.1994
			(0.3739*)		(3.8970*)		(0.3869*)
$\mu = 0.3$	σ_{max}	0	0.6783	0	0.4642	0	0.1724
	G_I	—	0.3350	—	1.7958	—	0.1907
			(0.3716*)		(3.8388*)		(0.3730*)

* Values calculated by $da = db = 0.0001$.

from large and suitably shaped flaws. Thus the fracture process in compression could be dominated by a system of severe flaws, which finally lead to macroscopic failure.

Since concrete is actually a heterogeneous material, aggregates may stop or change the direction of cracking. Furthermore, Shrive (1983) examined the effect of aggregate in the 3-D stress situation

and concluded that the tensile stresses developing at the tips of a spherical inclusion are largest when the inclusion is a void; however, aggregate particles may aid crack initiation and propagation around their surfaces.

There is still much controversy as to the very applicability of fracture mechanics principles to cementitious materials (Mindess, 1984). However, Glucklich (1963) stated that basically, concrete is not different to glass as was used in Griffith's pioneer work. Many metals are not homogeneous on the microstructural level; however, fracture mechanics deals quite adequately with the lack of microstructural homogeneity. The toughening mechanisms in quasi-brittle materials such as crack shielding, crack deflection, aggregate bridging and crack surface roughness-induced closure (Shah and Ouyang, 1993) may be incorporated in an 'effective' *R*-curve. Further, since crack initiation in compression may occur at various physical and geometrical inhomogeneities, consideration of the dominant mechanism for different materials appears practical. The current model may provide a first approximation for quasi-brittle materials.

A general procedure to quantify the effect of 3-D ellipsoidal flaw geometry on brittle fracture in compression is presented on the basis that flaws are known to occur in materials. The proposal provides an important mechanism for inducing large enough internal tensile stresses and energy release rates for Mode I fracture under compressive loads, and appears to give a basis for explaining the features of brittle fracture in compression common to many materials.

3-D flaw geometry has a pronounced effect on brittle fracture in compression and flaw size alone is not sufficient condition for crack initiation. Mode I crack initiation from flaws of different ellipsoidal geometries may occur at considerably different applied stress levels and the governing criterion for crack initiation may shift from the energy criterion to the stress criterion with increasing flaw size. For the compressive stress states considered here, the spherical, 'sausage' and whatever shapes occur between them, are the preferred shapes for crack initiation. For voids of similar size, the spherical void appears to be the most critical shape, and it has the potential to lead to short unstable crack propagation. Since the most critical void shape for compression is a sphere, the orientation of such a shaped void relative to the applied state stress state is of no consequence, confirming the relevance of the current model to crack initiation. Although flaw geometries in a material are statistical in character and involve great uncertainties and complexities in the analysis, particularly of composites like concrete, Mode I crack initiation always takes place first from the large and preferably shaped flaws. This will result in distributed cracking within the material. Failure of the specimen is eventually controlled by a number of cracks, their interaction and linkage. The presence of lateral confinement makes Mode I cracking less likely. For certain triaxial compressive loads, the stress criterion for Mode I crack initiation may not be satisfied and plastic behaviour as opposed to Mode I cracking may take place.

Although an ellipsoidal void might limit the sharpness of a flaw, the fact that it is 3-D as opposed to 2-D makes it favourable for the study of brittle fracture in compression. It is clear that much more work is required to predict crack profiles during crack extension. The current model can provide useful information on critical shapes and sizes of void for crack initiation in compressive stress states.

Acknowledgements

The financial support of the Natural Sciences and Engineering Research Council of Canada is gratefully acknowledged.

References

Adams, M., Sines G., 1978. Crack extension from flaws in a brittle material subjected to compression. Tectonophysics 49, 97–118.

Bazant, Z.P., Ozbolt, J., 1992. Compression failure of quasibrittle material: nonlocal microplane model. J. Engng Mech. 118, 540–556.

Birchall, J.D., Howard, A.H., Kendall, K., 1981. Flexural strength and porosity of cements. Nature 289, 388–390.

Brace, W.F., Silver, E., Hadley, K., Goetze, C., 1972. Cracks and pores: a closer look. Sci. 178, 162–164.

Bridgman, P.W., 1952. Studies in Large Plastic Flow and Fracture. McGraw-Hill Book Co., New York.

Brown, E.T., 1974, Fracture of rock under uniform biaxial compression. In: Advances in Rock Mechanics II, Part A, National Academy of Sciences, Washington, D.C., pp. 111–117.

Carter, B.J., 1992. Size and stress gradient effects on fracture around cavities. Int. J. Rock Mech. Rock Engng 25, 167–186.

Carter, B.J., Lajtai, E.Z., Yuan, Y., 1992. Tensile fracture from circular cavities loaded in compression. Int. J. Fracture 57, 221–236.

Chao, H.C., Van Vlack, L.H., 1965. Flow of steel near inclusion near deformation. Mater. Res. Standards 5, 611–613.

Durelli, A.J., 1981. Stress concentrations. In: Experimental Evaluation of Stress Concentrations and Intensity Factors. Martinus Nijhoff Publishers, The Hague, pp. 1–162.

Dyskin, A.V., Germanovich, L.N., Ustinov, K.B., 1993. Asymptotic solution for long cracks emanated from a pore in compression. Int. J. Fracture 62, 307–324.

El-Rahman, M., 1983. Stress concentration around ellipsoidal flaws in relation to the fracture of brittle materials. M.Sci. Thesis, The University of Calgary.

Evans, R.H., Marathe, M.S., 1968. Stress distribution around holes in concrete. Mater. Structures 1, 57–60.

Glucklich, J., 1963. Fracture of plain concrete. J. Engng Mech. 89, 127–138.

Gol'dshtein, R.V., Ladygin, V.M., Osipenko, N.M., 1974. A model of the fracture of a slightly porous material under compression or tension. Soviet Mining Sci. 10, 109.

Hobbs, D.W., 1971. Strength of concrete under combined stress. Cement Concr. Res. 1, 41–56.

Kotsovos, M.D., 1979. Fracture processes of concrete under generalised stress states. Mater. Struct. 12, 431–437.

Kumar, M.P., 1986. Concrete: Structure, Properties, and Materials, Prentice-Hall, Inc., Englewood Cliffs.

Kupfer, H., Hilsdorf, H.K., Rusch, H., 1969. Behaviour of concrete under biaxial stresses. J. ACI 66, 656–666.

Lajtai, E.Z., 1971. A theoretical and experimental evaluation of the Griffith theory of brittle fracture. Tectonophysics 11, 129–156.

Lajtai, E.Z., 1974. Brittle fracture in compression. Int. J. Fracture 10, 525–536.

Lajtai, E.Z., Carter, B.J., Ayari, M.L., 1990. Criteria for brittle fracture in compression. Engng Fracture Mech. 37, 59–74.

Madenci, E., 1991. Slightly open, penny-shaped crack in an infinite solid under biaxial compression. Theoret. Appl. Fracture Mech. 16, 215–222.

Madenci, E., Klemm, W., 1992. Compression-induced failure of a glassy material with a crack-like defect. Engng Fracture Mech. 41, 443–452.

Mazars, J., 1986. A description of micro- and macroscale damage of concrete structures. Engng Fracture Mech. 25, 729–737.

Mindess, S., 1984. Fracture toughness testing of cement and concrete. In: Fracture Mechanics of Concrete: Material Characterization and Testing. Martinus Nijhoff Publishers, The Hague, pp. 67–110.

Murrell, S.A.F., Digby, P.J., 1970. The theory of brittle fracture initiation under triaxial stress conditions—I. Geophys. J. Astr. Soc. 19, 309–334.

Myer, L.R., Kemeny, J.M., Zheng, Z., Suarez, R., Ewy, R.T., Cook, N.G.W., 1992. Extensile cracking in porous rock under differential compressive stress. Appl. Mech. Rev. 45, 263–280.

Nemat-Nasser, S., Horii, H., 1982. Compression-induced nonplanar crack extension with application to splitting, exfoliation, and rockburst. J. Geophys. Res. 87, B8, 6805–6821.

Neville, A.M., 1981. Properties of Concrete, 3rd Ed. Pitman, London.

Page, A.W., 1982. An experimental investigation of the biaxial strength of brick masonry. In: Proceedings of the 6th Int. Brick Masonry Conf., Rome, pp. 3–15.

Paul, B., Mirandy, L., 1976. An improved fracture criterion for three-dimensional stress states. J. Engng Mater. Technol. 98, 159–163.
Peng, S., Podnieks, E.R., 1972. Relaxation and behaviour of failed rock. Int. J. Rock Mech. Min. Sci. 9, 699–712.
Peterson, R.E., 1974. Stress Concentration Factors. John Wiley & Sons, New York.
Raju, N.K., 1970. Effect of stress concentrations on the static and fatigue strength of concrete in compression. Mater. Structures 3, 85–89.
Rice, J.R., Drucker, D.C., 1967. Energy changes in stressed bodies due to void and crack growth. Int. J. Fracture Mech. 3, 19–27.
Roy, D.M., Gouda, G.R., 1975. Optimization of strength in cement pastes. Cement Concr. Res. 5, 153–162.
Sadowsky, M.A., Sternberg, E., 1949. Stress concentration around a triaxial ellipsoidal cavity. J. Appl. Mech. 16, 149–157.
Sammis, C.G., Ashby, M.F., 1986. The failure of brittle porous solids under compressive stress states. Acta Metall. 34, 511–526.
Savin, G.N., 1961. Stress Concentration around Holes. Pergamon Press, London.
Shah, S.P., Ouyang, C., 1993. Toughening mechanisms in quasi-brittle materials. J. Engng Mater. Technol. 115, 300–307.
Shrive, N.G., 1983. Compression testing and cracking of plain concrete. Mag. Concr. Res. 35, 27–39.
Shrive, N.G., El-Rahman, M., 1985. Understanding the cause of cracking in concrete: a diagnostic aid. Concr. Intl. 7, 39–44.
Slate, F.O., 1983. Microscopic observation of cracks in concrete, with emphasis on techniques developed and used at Cornell University. In: Fracture Mechanics of Concrete, Elsevier Science Publishers B.V., Amsterdam, pp. 75–84.
Southwell, R.V., Gough, H.J., 1926. On the concentration of stress in the neighbourhood of a small spherical flaw; and on the propagation of fatigue fracture in 'statistically isotropic' materials. Phil. Mag. 7, 71–97.
Sprunt, E.S., Brace, W.F., 1974. Direct observations of microcavities in crystalline rocks. Int. J. Rock Mech. Min. Sci. 11, 139–150.
Van Vlack, L.H., 1989. Elements of Materials Science and Engineering, 6th ed. Addison-Wesley Publishing Company, Inc., Reading.
Vile, G.W.D., 1968. The strength of concrete under short-term static biaxial stress. In: Proc. Int. Symp. on the Structure of Concr., Cement and Concrete Association, London, pp. 275–288.
Yuan, Y.G., Lajtai, E.Z., Ayari, M.L., 1993. Fracture nucleation from a compression-parallel, finite-width elliptical flaw. Int. J. Rock Mech. Min. Sci. 30, 873–876.
Wang, E.Z., Shrive, N.G., 1993. On the Griffith Criteria for brittle fracture in compression. Engng Fracture Mech. 46, 15–26.
Wang, E.Z., Shrive, N.G., 1994. A 3-D approach to the calculation of the energy release rate in some fracture problems. Int. J. Fracture 66, 71–89.
Zaitsev, J.V., 1971. Deformation and failure of hardened cement paste and concrete subjected to short term load. Cement Concr. Res. 1, 123–137 (in Russian).
Zaitsev, Y.B., 1983. Crack propagation in a composite material. In: Fracture Mechanics of Concrete. Elsevier Science Publishers B.V., Amsterdam, pp. 251–300.